Journal of Materials Chemistry

Dynamic Article Links

Cite this: J. Mater. Chem., 2011, 21, 9538

www.rsc.org/materials

PAPER

Relationship between supramolecular assembly and charge-carrier mobility in perylenediimide derivatives: The impact of side chains†

Falk May,[a] Valentina Marcon,[b] Michael Ryan Hansen,*[a] Ferdinand Grozema[c] and Denis Andrienko*[a]

Received 1st February 2011, Accepted 20th April 2011
DOI: 10.1039/c1jm10500k

Discotic mesophases are known for their ability to self-assemble into columnar structures which serve as semiconducting molecular wires. Charge-carrier mobility along these wires strongly depends on molecular packing which is controlled by intermolecular interactions. Using solid-state NMR and molecular dynamics simulations we relate how conformations of alkyl and glycol side chains affect helical pitch and angular distribution of molecules within the columnar structures of perylenediimide derivatives. Using the high-temperature limit of Marcus theory we then establish a link between the secondary structure and charge-carrier mobility. Simulation results are compared to pulse-radiolysis time-resolved microwave conductivity measurements. We conclude that for achieving high charge-carrier mobilities in discotics, side chains with specific interactions are required in order to minimize the translational and orientational molecular disorder in the columns.

1 Introduction

Among the advantages of organic semiconductors are their synthetically tunable electronic structure, their self-assembling abilities, and their ease of processing. Doped[1–3] and neutral soluble[4,5] conjugated polymers as well as vapor-deposited[6,7] and soluble[8–10] small organic molecules are currently utilized as building blocks for various electronic and optoelectronic devices. Discotic liquid crystals represent a subset of soluble self-organizing compounds displaying columnar molecular arrangement. The overlap of the π-orbitals of the neighboring molecules allows for one-dimensional transport of charge carriers along the columns.[8,11–15] Local charge-carrier mobilities up to 1 $cm^2 V^{-1} s^{-1}$ can be achieved by systematically varying the substituents and processing.[16–18] Perylenediimide (PDI) derivatives form a particularly interesting class of discotics, since compounds based on these derivatives are some of the best and most frequently used n-type semiconductors,[12,19] even though their electron and hole mobilities are rather similar.[20] Mobilities up to 0.6 $cm^2 V^{-1} s^{-1}$ have been reported for thin PDI films.[21,22] PDI derivatives have already been applied in different areas of organic electronics, such as all-organic solar cells[13,23–25] and field-effect transistors.[12,26] They can self-assemble in structures with different packing motifs,[27] which also results in different charge mobilities.[28] The self-organization can be controlled by introducing hydrogen bonding,[29] metal-ion coordination,[30] or by changing the geometry of the side groups.[31,32]

Since high charge-carrier mobility is essential for the majority of applications, significant efforts have been directed at its improvement, for example by varying the chemical structure.[33,34] It has been concluded, however, that optimizing the electronic structure alone is not sufficient, since the material morphology, which heavily depends on both chemical structure and processing, can alter charge mobility by orders of magnitude.[35,36] This suggests that the following steps are required for compound design: synthesis of a new compound, optimization of processing conditions, morphology characterization, and finally measurements of the mobility.[18,37–41] Reiterating this procedure for a set of compounds, one might be able to formulate a set of empirical rules, or structure-processing-property relationships. In practice, however, finding such relationships has been so far very difficult. It is often not obvious whether the improvement comes from a better electronic structure or a superior morphology, since both are affected by changes in the chemical structure.

A particularly difficult problem is to characterize partially disordered material morphologies with a high level of detail. Routinely employed experimental techniques are wide-angle X-ray scattering (WAXS)[41–43] and solid-state nuclear magnetic resonance (NMR).[41,44–46] Both methods provide *averages* over the molecular ensemble and, as such, do not contain full information about the *distributions* of molecular positions and orientations. At the same time, charge dynamics of partially ordered semiconductors is sensitive to the molecular arrangement on all length scales.[47,48] Indeed, transfer integrals and charge hopping rates strongly depend on the chemical

[a]*Max Planck Institute for Polymer Research, Ackermannweg 10, 55128 Mainz, Germany. E-mail: hansen@mpip-mainz.mpg.de; denis.andrienko@mpip-mainz.mpg.de*
[b]*Center of Smart Interfaces, Petersen str. 32, 64287 Darmstadt, Germany*
[c]*DelftChemTech, Delft University of Technology, Juliana laan 136, 2628 BL Delft, The Netherlands*

† Electronic supplementary information (ESI) available: details of molecular dynamics and charge transport simulations, solid state NMR and pulse-radiolysis time-resolved microwave conductivity measurements. See DOI: 10.1039/c1jm10500k

composition and *local* molecular ordering, while the global charge-carrier pathway is determined by the *large scale* morphology and presence of defects. In this situation, modeling becomes a necessity: it assists in identifying correct molecular packing motifs[18,49–51] quantifies the degree of local disorder, and links both of these to the charge-carrier mobility.[18,47,48,52–61] In our previous work we have established a link between charge mobility and morphology for the derivatives of hexabenzocoronene,[48,50] addressed the structure-mobility relations for the heptyloctyl substituted perylene tetracarboxdiimide derivative, and designed a new class of triangularly-shaped discotics[18] with high charge-carrier mobility. In all cases, the morphology of the materials was characterized using molecular dynamics simulations guided by the WAXS and NMR data analysis. Even though we have been able to establish a relation between the local disorder and charge mobility, no definitive conclusion was made about the role of the side chains, *e. g.* why different side chains lead to different supramolecular (in this case helical) packing motives. Such understanding is of course required for rational compound design, since the local packing motif as well as its quality have a significant effect on charge transport.

In this work we compare the supramolecular arrangement of two PDI derivatives, with alkyl ($C_{8,7}$–PDI) and tri-ethylene-glycol (TEG–PDI) side chains, the chemical structure of which is shown in Fig. 1a,b. To do this, we first analyze the experimental results from solid-state NMR and WAXS data and correlate the deduced molecular arrangement with the results of molecular dynamics (MD) simulations. Analyzing the MD snapshots we relate packing of side chains to the supramolecular helical arrangement of molecules in a column. Finally, we calculate electronic couplings between conjugated cores of neighboring molecules and use high-temperature non-adiabatic limit of Marcus theory to calculate the charge hopping rates between them. Charge-carrier mobility for electrons and holes is then obtained by solving a linearized master equation for occupation probabilities. Simulation results are compared to pulse-radiolysis time-resolved microwave conductivity (PR-TRMC) mobility measurements. Eventually, structure-mobility relationships are formulated.

2 Phase behavior, packing, and local molecular dynamics from solid-state NMR

To investigate the self-assembled packing motifs and local molecular dynamics of the two PDI derivatives we have employed a number of advanced solid-state NMR experiments.[63–66] These experiments probe the local molecular conformations, averaged over the whole sample, through the isotropic chemical shift (δ_{iso}) and correlation of these through the space-dependent dipole–dipole coupling.[67,68] Information about the local molecular dynamics can also be achieved by monitoring the effective ^{13}C-^{1}H heteronuclear dipolar couplings.[69] In particular, the δ_{iso} for ^{1}H is known to be a sensitive probe with respect to π–π stacking effects,[44,45] hydrogen bonding,[70,71] and, as we have recently shown, also to specific pitch angles between successive PDI molecules within the molecular stacks.[46]

A detailed characterization of $C_{8,7}$–PDI employing solid-state NMR, MD simulations, and WAXS have previously been performed[46,72] and for this reason, only a short summary of these findings will be given here. The $C_{8,7}$–PDI molecules are π–π stacked and organized in columns with a low pitch angle of about 20–45°. This information was derived from the observation of a strong inter-molecular contact between the branching protons of the attached side chains for successive $C_{8,7}$–PDI molecules, yielding a distance of 3.7 ± 0.1 Å. Moreover, the chemical shift for this particular proton (~4.8 ppm) indicates that this is

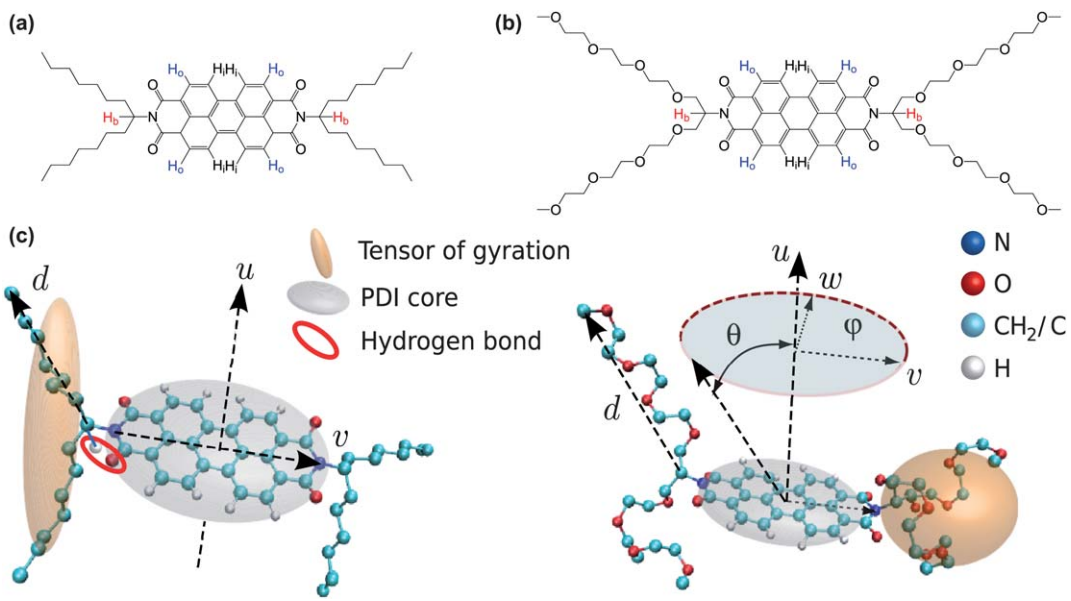

Fig. 1 (a) $C_{8,7}$–PDI, alkyl side chain and (b) TEG–PDI, tri-ethylene-glycol (TEG) side chain. (c) Sketch of the two PDI derivatives: side chains are displayed using united atom representation except for the branching C-atom. The orientation of the conjugated core defines the coordinate systems given by vectors $\boldsymbol{v}$ (connects the two N-atoms in the molecular plane), $\boldsymbol{u}$ (normal to the molecular plane), and $\boldsymbol{w} = \boldsymbol{u} \times \boldsymbol{v}$. Angles θ and ϕ are polar and azimuthal angles of the end-to-end vector d in this coordinate system. Ellipsoids depict tensors of gyration for each pair of side chains. Labels for different H atoms are used for dynamical order parameters in Table 1.

hydrogen bonded and thereby coordinated to the carbonyls of either side of the PDI core, as indicated in Fig. 1c. Such an intramolecular hydrogen bond, although quite unusual since it involves a CH group and a carbonyl, is expected to be important with respect to how the attached side chains pack and organize themselves between the individual columns. We note that this kind of hydrogen bond has previously been observed in other systems using solid-state NMR and quantified with respect to its impact on the proton chemical shift of the methine group by theoretical calculations.[73,74] Another example of this particular hydrogen bond is the perylenemonoimide (PMI) system where the attachment of identical branched side chains ($C_{8,7}$) leads to a larger stacking angle between successive PMIs, which allows for the existence of two fractions of hydrogen-bonded side-chain species.[75] Finally, the $C_{8,7}$–PDI core part was observed to be rather rigid as identified from site specific dynamical order parameters S close to unity, indicating that the columnar packing of $C_{8,7}$–PDI is rather stable.

Replacing the alkyl side chains with TEG at the branching point has a dramatic effect on both the thermotropic behavior and columnar packing of the PDI molecules as can be observed from Fig. 2. From Fig. 2c the thermotropic behavior of TEG–PDI can easily be followed and transition temperatures at ~53 and ~130 °C can be identified, corresponding to the phase transitions from crystalline (Cr) to liquid crystalline (LC) and from LC to the isotropic phase, respectively. In our previous work we have focused on the LC phase only and it was shown that the LC phase of TEG–PDI includes a cooperative motion along the columns where the TEG–PDI molecules are packed with a pitch angle of 90°.[62] As a consequence of the increased mobility along the columnar axis, the linebroadening effects from the homo-nuclear proton-proton dipolar couplings are significantly reduced. This leaves the ^{1}H resonances mainly influenced by π–π packing effects and allows for the assignments shown in Fig. 2a and d.

Cooling TEG–PDI from the LC phase to the Cr phase gives the 2D solid-state NMR spectra shown in Fig. 2b and e. From both of these spectra it is apparent, that a freezing in of the TEG chains has a large impact on the spectral resolution which can be achieved. This is most clearly observed by a comparison of Fig. 2a and b which also reveals, that δ_{iso} for the TEG chains is shifted from ~4.6 to ~3.4 ppm in LC and Cr phases, respectively.

To reveal what the impact of freezing of the TEG chains is with respect to packing the 2D ^{13}C{^{1}H} correlation spectrum in Fig. 2e is very useful. From this 2D spectrum, the broad 1D spectrum of ^{1}H chemical shifts is now spread according to their carbon bonding partner, giving a much improved resolution. Clearly, the packing of TEG–PDI molecules in the Cr phase is quite different from the LC phase, since six distinct ^{13}C sites with attached protons can be observed. These sites belong to different packing motifs in the columns and comes as a result of different pitch angles as shown in our previous work.[46] Based on this, the different sites can be grouped together as illustrated in Fig. 2e. With this in mind the packing of TEG–PDI can be understood.

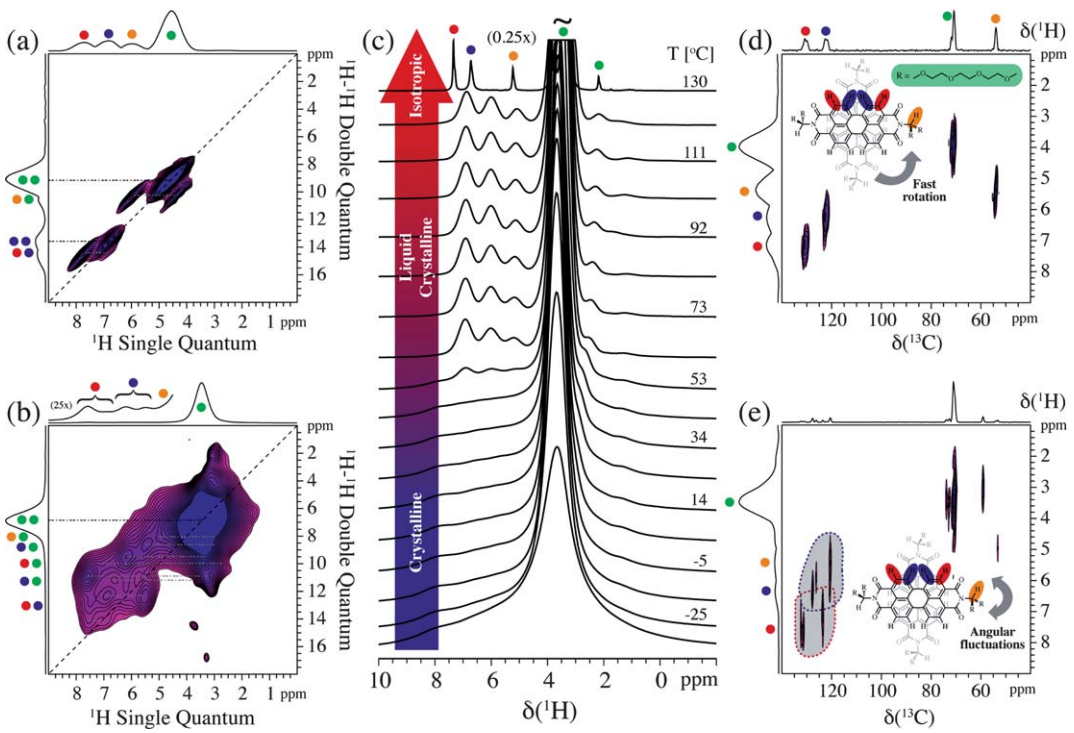

Fig. 2 Phase behavior and supramolecular assembly of TEG–PDI. (a) and (b) 2D ^{1}H-^{1}H DQ-SQ correlation spectra recorded at 20.0 T using a DQ excitation/reconversion of two rotor periods for a spinning frequency of 30.0 kHz. (c) Variable temperature ^{1}H MAS NMR spectra recorded at 16.5 T illustrating the thermotropic behavior of TEG–PDI. (d) and (e) 2D ^{13}C{^{1}H} REPT-HSQC spectra recorded at 20.0 T using a REDOR recoupling time of two rotor periods and a spinning frequency of 25.0 kHz. The upper spectra shown in (a) and (d) have been recorded in the liquid-crystalline phase for TEG–PDI at 92 °C and the lower spectra in (b) and (e) have been recorded at 14 °C in the crystalline (or "frozen") phase of TEG–PDI. The insets in (d) and (e) display the color scheme employed for assignment along with the packing (as seen from above) and molecular dynamics.[62]

The main packing motif, showing the largest spread in chemical shift, is packed with a pitch angle of 90° as also identified from WAXS measurements.[62] The two remaining packing motifs on the other hand indicate that these are stacked with pitch angles less than 90°. This immediately raises two questions. How can such a complex packing be understood and what is the role of the attached TEG side chains? To answer these questions a deeper understanding of the morphology of the TEG–PDI system in its crystalline state is required. Fortunately, the MD simulations performed in this work give access to realistic packing scenarios and these will form the basis for understanding the complex packing present in $C_{8,7}$–PDI and TEG–PDI.

Before going in detail about the different morphologies and packing motifs it is illustrative to compare the order parameters obtained experimentally for $C_{8,7}$–PDI and TEG–PDI from solid-state NMR experiments[46,62] with those calculated based on MD simulations.[72] The dynamical order parameter S is related to the mobility of a moiety of interest. From MD this can be computed as

$$S = \left\langle \frac{1}{N}\sum_{i=1}^{N}\left(\frac{3}{2}(M_i \cdot m_i)^2 - \frac{1}{2}\right)\right\rangle, M_i = \langle m_i \rangle, \quad (1)$$

where <…> denotes time average, N is the number of molecules in the system, m_i is the vector along the C–H_x group of interest, H_i, H_o, H_b in our particular case, see Fig. 1a for the notations.

Calculated dynamical order parameters are summarized together with the NMR results in Table 1. As an example for the $C_{8,7}$–PDI case a value of $S = 0.91$ ($T = 300$ K) is calculated for the inner-most core protons of the PDI core.[72] This is in good agreement with the dynamical order parameter of $S \sim 0.9$ determined from solid-state NMR experiments[46] and shows that the columnar system based on $C_{8,7}$–PDI is quite stable even on small time scales, as in the case of the MD simulations performed in this work. For the TEG–PDI case the experimentally determined order parameters are on the order of $S \sim 0.5$ in both the LC and Cr phase (see Table 1). This reduction by about a factor of 2 from a completely rigid case could be explained by the presence of cooperative motion and local fluctuations of the columnar-packed molecules in the LC and Cr phases, respectively, as indicated in Fig. 2d and e.[62] From the MD simulations performed for TEG–PDI in this work, values in the range of 0.8–0.9 for S are obtained for the PDI core part of TEG–PDI (see Table 1). The discrepancy between experimental and calculated order parameters for TEG–PDI mainly reflect that the different kind of motions occurring in the two different thermodynamic phases of TEG–PDI are on time scales longer than what is sampled in the MD simulations (ns) as compared to that detected during the solid-state NMR experiments (ms). Thus, the MD simulations performed for TEG–PDI should mainly be considered as a *static snapshot* of the morphology which, however, still can be used to interpret the charge-carrier mobility of the TEG–PDI-system, since this occurs on a much faster time scale (sub-nanoseconds). In addition to the dynamic order parameter we have computed an orientational order parameter Q as the largest eigenvalue of

$$Q_{\alpha\beta} = \left\langle \frac{1}{N}\sum_{i=1}^{N}\left(\frac{3}{2}u_\alpha^{(i)}u_\beta^{(i)} - \frac{1}{2}\delta_{\alpha\beta}\right)\right\rangle, \quad (2)$$

$Q = 1$ implies perfect alignment of the unit vectors $\boldsymbol{u}$ (see Fig. 1) and $Q = 0$ corresponds to an isotropic angular distribution. Both derivatives show strong nematic order as can be seen in Table 1.

Table 1 Dynamic order parameters S for the different core C–H moieties determined from MD simulations (see eqn (1)) and 2D rotor-encoded solid-state NMR and the corresponding orientational order parameter Q from MD (see eqn (2)). Experimental uncertainties are ±0.1

Method	PDI	T/K	$S(CH_o)$	$S(CH_i)$	$S(CH_b)$	Q
NMR[46]	$C_{8,7}$–PDI	300	0.9	~1	0.9	
NMR[62]	TEG–PDI	303	0.46	0.43	0.48	
NMR[62]	TEG–PDI	373	0.48	0.48	0.52	
MD[72]	$C_{8,7}$–PDI	300	0.91	0.86	0.96	0.90
MD	TEG–PDI	300	0.93	0.88	0.98	0.95
MD	TEG–PDI	400	0.89	0.84	0.96	0.94

3 Molecular ordering: Simulations

Atomistic molecular dynamics simulations were employed in order to link the side-chain packing and the molecular arrangement within columns. All systems consisted of 960 PDI molecules stacked in 16 columns of 60 molecules each. Force-field parameters and simulation details can be found in the Supporting Information.†[18,72]

Initial configurations were prepared using an orthorhombic unit cell with $a = 22$ Å, $b = 17$ Å, and $c = 3.5$ Å for $C_{8,7}$–PDI,[72] and a hexagonal lattice with $a = b = 23$ Å, $c = 3.4$ Å for TEG–PDI.[62] Systems were equilibrated at 300 K for 40 ns using the GROMACS package[76] while the VOTCA package[77] was used to analyze the MD trajectories. Different initial pitch angles were used and we found that $C_{8,7}$–PDI converges to an average pitch angle of 40°, and TEG–PDI to 90°, in agreement to our previous results.[72] The histograms of the pitch angle α between neighboring molecules are shown in Fig. 3a. A narrow distribution with a maximum around 40° is found for $C_{8,7}$–PDI while for TEG–PDI the distribution is much broader and is centered around 90°. This agrees with the NMR results of 20°–45° for $C_{8,7}$–PDI[46] and 90° for TEG–PDI[62] as was mentioned in the last section. Furthermore, the broad pitch angle distribution for TEG–PDI shows indications of the packing motifs revealed by solid-state NMR. In our previous work the width of the distribution was estimated to be ±40° from site-specific ^{13}C-^{1}H dipolar couplings[62] which is in excellent agreement with simulation results. Intermolecular distances have a narrow distribution for both compounds which has maximum around 3.6 Å, as shown in Fig. 3b.

To understand the difference in molecular packing of the two PDI derivatives we analyzed conformations of their side chains. This was done with the help of the end-to-end vector $\boldsymbol{d}$ connecting the branching C-atom and the end of the side chain, as illustrated in Fig. 1c. The distributions of the length of this vector, $d = |\boldsymbol{d}|$, are shown in Fig. 3b. The narrower distribution for alkyl side chains suggests that they are more rigid and stretched out as compared to the TEG side chains, which is due to steric repulsion of hydrogens attached to sp^3-hybridized carbons.

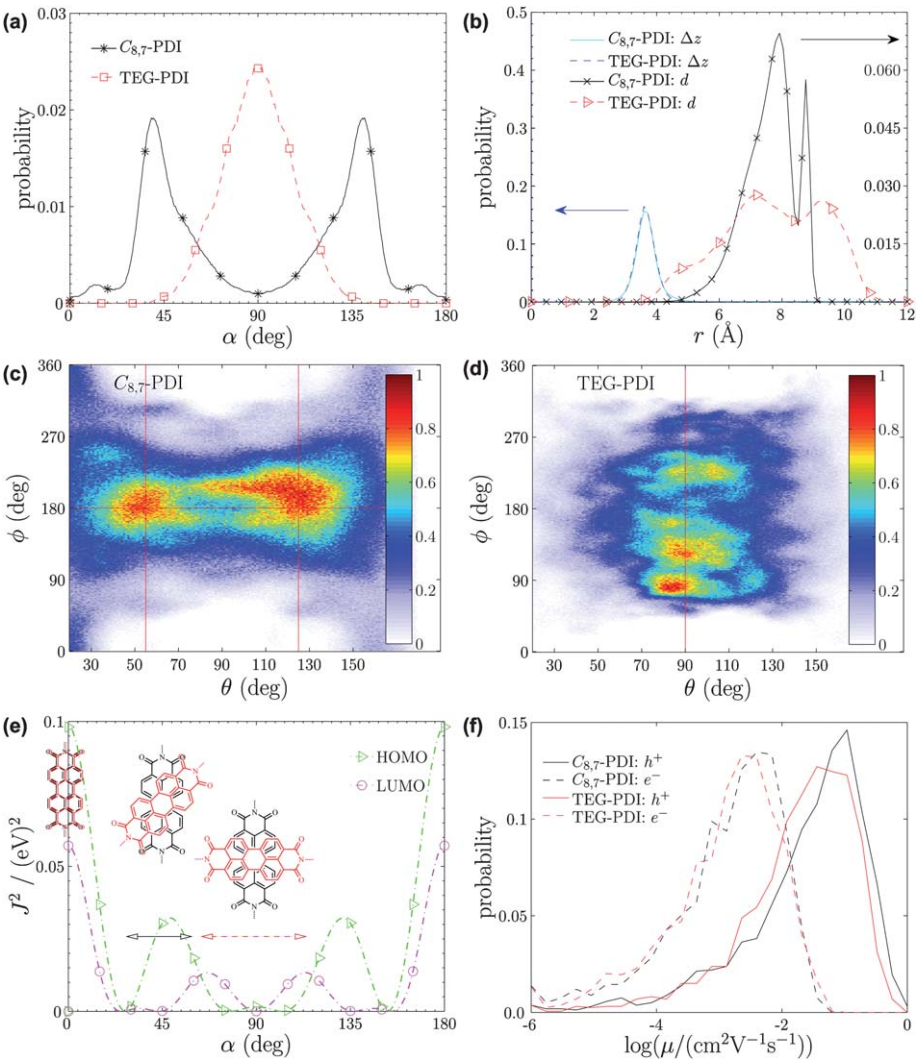

Fig. 3 (a) Histograms of the helical pitch angle of neighboring molecules, α. (b) Histograms of the intermolecular distance Δz and length d of the four side chains (see Fig. 1). The narrower distribution of d for $C_{8,7}$–PDI which has less atoms shows that alkyl side chains are more rigidly stretched out and TEG side chains are more flexible. (c) and (d) Orientation of the end-to-end distance d for alkyl and TEG side chains with respect to the core (see Fig. 1 for definitions). The hydrogen bond near the branching C-atom defines the direction of the stiff alkyl side chain to point out of the molecular plane $\theta \approx 55°$ (red vertical line) while the more flexible TEG side chains can average out the direction given by the hydrogen bond and can rest in the molecular plane $\theta \approx 90°$. This results in different pitch angles of $\alpha = 40(90)°$ for $C_{8,7}$–PDI(TEG–PDI) as explained below. (e) HOMO-HOMO (triangles) and LUMO-LUMO (circles) transfer integrals for two isolated molecules at a distance of $\Delta z = 3.6$ Å as a function of the relative pitch angle α. The widths of the distributions of pitch angles shown in Fig. 3a are indicated using black and red arrows for $C_{8,7}$–PDI and TEG–PDI, respectively. Minima of J^2_{LUMO} occur near maxima of these distributions at $\alpha = 40°$ ($C_{8,7}$–PDI) and $\alpha = 90°$ (TEG–PDI). (f) Distributions of charge carrier mobilities for electrons and holes for $C_{8,7}$–PDI and TEG–PDI. Hole mobilities are larger for both derivatives.

Mean values of the two distributions are similar, $\bar{d} = 7.6$ Å for $C_{8,7}$–PDI and 7.7 Å for TEG–PDI, in spite of the fact that the alkyl side chain has less atoms than the TEG side chain. This observation is further confirmed by comparing the eigenvalues of the tensor of gyration for the two combined branches of side chains (see Fig. 1c). $C_{8,7}$–PDI has a ratio of eigenvalues (in nm^2) 43 : 6 : 1 in contrast to 17 : 3 : 1 for TEG–PDI, indicating again that the TEG side chain is more flexible than the alkyl one. The tensors of gyration are sketched in Fig. 1c.

The orientation of the vector $\boldsymbol{d}$ is characterized using two-dimensional histograms in the ϕ,θ coordinates, introduced in Fig. 1, and are shown in Fig. 3c and d. Alkyl side chains stick out of the molecular plane by $\pm 35°$ since the distribution is centered around $\theta = 55°$ and 125°. Hence, on average the side chains point away from the plane of the core. In contrast, the TEG side chains reside in the molecular plane, since their distribution is centered around $\theta = 90°$.

The observed conformational differences can be easily linked to the chemical structure. Simulation results as well as the NMR data suggest[46] that a hydrogen bond is formed between the H-atom attached to the branching C-atom of the side chain and the O-atom of the core (see Fig. 1). Due to the tetrahedral structure around the branching C-atom, the first C-atoms in the two sidearms will therefore be out of the molecular plane. This direction is maintained in the case of $C_{8,7}$–PDI because of the rigid nature of alkyl side chains. For more flexible TEG–PDI

chains, the direction imposed by the first C-atoms averages out and the side chains reside in the molecular plane.

Summarizing the MD results, one can conclude that the pitch angle of $\alpha = 90°$ for TEG–PDI is a consequence of a steric repulsion of the TEG side chains belonging to the *neighboring* molecules. For $C_{8,7}$–PDI the alkyl side chains stick out of the molecular plane due to the hydrogen bond formation. Due to their larger extension, steric repulsion exists not only between the side chains of nearest neighbors but also the *next* nearest neighbors. Therefore the pitch is reduced to $\alpha = 40°$, which ensures the best side chain packing.

4 Charge-carrier mobility

With the atomistic morphologies at hand, we can now calculate hole and electron mobilities along the columns. To do this, charge hopping rates for neighboring molecules i and j were calculated using the high-temperature limit of Marcus theory[78,79]

$$\omega_{ij} = \frac{J_{ij}^2}{\hbar}\sqrt{\frac{\pi}{\lambda k_B T}}\exp\left(-\frac{\lambda}{4k_B T}\right), \quad (3)$$

where k_B is Boltzmann's constant, $\hbar$ is Planck's constant, λ is the reorganization energy, and J_{ij} is the corresponding transfer integral. Centers of mass of molecules were used as hopping sites. Charge-carrier mobilities were obtained by solving a linearized master equation for one-dimensional transport.[47,48,80,81] A description of the master equation approach and details on how the diabatic states were constructed as well as how transfer integrals were calculated are given in the Supporting Information.†

The key parameters entering eqn (3) are the transfer integral J_{ij} and the reorganization energy λ. We will first discuss the contribution of the internal reorganization energy which was calculated using B3LYP hybrid functional and 6-311g(d,p) basis set. The value for holes, $\lambda_h = 0.14$ eV, is significantly smaller than the value for electrons, $\lambda_e = 0.24$ eV, leading to about four times higher rates for holes than for electrons (for details on this and the details on the method we use to obtain reorganization energies see the Supporting Information†).

The other contribution to the hopping rate comes from the transfer integral J_{ij}. It is related to the overlap of orbitals used to construct diabatic states (HOMO for holes and LUMO for electrons) and hence is very sensitive to relative orientations and positions of neighbors. The distribution of the center of mass distances between neighbors in a column, shown in Fig. 3b, is rather narrow and peaked around $\Delta z = 3.6$ Å. This value is in agreement with the WAXS data.[62,72] Hence, the variation of transfer integrals is mostly due to the change in relative orientations of neighboring molecules. The dependence of the transfer integrals for electrons and holes on the relative orientation angle α is shown in Fig. 3a. For convenience, the widths of the distributions of the angle α are also shown. From Fig. 3e one might anticipate that average electronic coupling for electrons is much smaller than that for holes, since the minima of the J_{LUMO} are close to the maxima of the angle distributions. Since the transport is effectively one-dimensional, the charge carrier is very likely to encounter a very small transfer integral within the column, which will lead to small charge carrier mobilities. Indeed, the averaged mobilities, given in Table 2, show that hole transport is roughly twenty times more efficient than electron transport for both derivatives. This is unexpected since PDI are known as n-type semiconductors,[12,19] although it has been shown experimentally that their electron and hole mobilities are rather similar.[20]

Table 2 Simulated and experimental mobilities, in $cm^2\ V^{-1}\ s^{-1}$. Values for electron and hole mobilities for both PDI derivatives are obtained by averaging over 16 columns in 1000 MD snapshots of a 40 ns long trajectory. We also show combined electron and hole mobilities which can be directly compared to measured PR-TRMC mobilities

	$C_{8,7}$–PDI	TEG–PDI
μ_h	0.086	0.071
μ_e	0.004	0.004
$\mu_e + \mu_h$	0.09	0.075
$\mu_{PR-TRMC}$	0.15	0.09

The slightly smaller hole mobility in TEG–PDI shown in Table 2 is due to the broad pitch angle distribution that covers the minimum of the HOMO-HOMO overlap around 80°. The narrower distribution for $C_{8,7}$–PDI only covers the minima with its tails, as can be seen in Fig. 3a and e. Broad distributions of the pitch angle result in broad distributions of charge mobilities in columns, which are shown in Fig. 3f.

The sum of the electron and hole mobilities can be directly compared to the mobility measured by pulse-radiolysis time-resolved microwave conductivity (PR-TRMC) technique. The details of this technique are described in the Supporting Information.† Note that Marcus theory tends to slightly overestimate the value of the mobility measured by the PR-TRMC technique. For PDI, however, our averaged estimates are smaller than the experimentally measured mobilities. This implies that the length of a column comprised of 60 molecules exceeds the distances sampled by the PR-TRMC technique, which normally probes only 10–20 molecules.[72] As a result, PR-TRMC is relatively insensitive to occasional stacking defects, while they are accounted for in simulations.

5 Conclusions

By combining MD simulations and NMR experiments we were able to link the value of the helical pitch to side chain conformations for two perylenediimide derivatives. The alkyl side chains prefer a linearly stretched out conformation with the end-to-end vector pointing out of the molecular plane. As a result, not only the nearest neighbors, but also the next nearest neighbors interact with each other which results in a pitch angle of 40°. The glycol side chains are more flexible and reside in the molecular plane. This leads to a much broader distribution of the pitch angle centered around 90°.

Since the minima of the LUMO-LUMO electronic coupling occur close to 40° and 90°, electron transport for both derivatives is less favorable as compared to hole transport. This is further enhanced by a smaller reorganization energy of holes as compared to electrons.

Comparing hole transport in both derivatives we find that minima of transfer integrals occur at pitch angles which are less probable in the case of $C_{8,7}$–PDI as compared to TEG–PDI. Computed mobilities, however, do not show a big difference

between hole mobilities in $C_{8,7}$–PDI and TEG–PDI. We therefore conclude that, in order to obtain maximal charge-carrier mobilities, it is not sufficient to match the average local molecular order induced by the side chains with maxima of the transfer integrals. It is also important to make the corresponding distributions as narrow as possible compared to the window determined by the closest minima of the transfer integral. The immediate implication for the compound design is that the side chains should assist the self-assembling process not only *via* "soft" entropic interactions, but also *via* stronger specific interactions, such as hydrogen bonding.

Acknowledgements

This work was partially supported by DFG *via* IRTG program between Germany and Korea, grants AN 680/1-1 and SPP1355, and the BMBF program MESOMERIE. V.M. and D.A. acknowledge the Multiscale Materials Modeling Initiative of the Max Planck Society. V.M. acknowledges the Alexander von Humboldt foundation. MRH acknowledges financial support from the Carlsberg Foundation and valuable discussions and continuing support from H. W. Spiess. We are grateful to Björn Baumeier and Mara Jochum for critical reading of the manuscript.

References

1 G. Wegner, *Angew. Chem., Int. Ed. Engl.*, 1981, **20**, 361–381.
2 D. Kumar and R. Sharma, *Eur. Polym. J.*, 1998, **34**, 1053–1060.
3 A. MacDiarmid, *Rev. Mod. Phys.*, 2001, **73**, 701–712.
4 P. Blom and M. Vissenberg, *Mater. Sci. Eng., R*, 2000, **27**, 53–94.
5 R. Kroon, M. Lenes, J. Hummelen, P. Blom and B. De Boer, *Polym. Rev.*, 2008, **48**, 531–582.
6 A. Murphy and J. Frechet, *Chem. Rev.*, 2007, **107**, 1066–1096.
7 J. Roncali, *Chem. Rev.*, 1997, **97**, 173–205.
8 J. Wu, W. Pisula and K. Müllen, *Chem. Rev.*, 2007, **107**, 718–747.
9 P. Leclere, M. Surin, P. Viville, R. Lazzaroni, A. Kilbinger, O. Henze, W. Feast, M. Cavallini, F. Biscarini, A. Schenning and E. Meijer, *Chem. Mater.*, 2004, **16**, 4452–4466.
10 P. Leclere, M. Surin, P. Jonkheijm, O. Henze, A. Schenning, F. Biscarini, A. Grimsdale, W. Feast, E. Meijer, K. Müllen, J. Bredas and R. Lazzaroni, *Eur. Polym. J.*, 2004, **40**, 885–892.
11 D. Adam, P. Schuhmacher, J. Simmerer, L. Haussling, K. Siemensmeyer, K. H. Etzbach, H. Ringsdorf and D. Haarer, *Nature*, 1994, **371**, 141–143.
12 G. Horowitz, F. Kouki, P. Spearman, D. Fichou, C. Nogues, X. Pan and F. Garnier, *Adv. Mater.*, 1996, **8**, 242.
13 L. Schmidt-Mende, A. Fechtenkotter, K. Müllen, E. Moons, R. H. Friend and J. D. MacKenzie, *Science*, 2001, **293**, 1119–1122.
14 F. Hoeben, P. Jonkheijm, E. Meijer and A. Schenning, *Chem. Rev.*, 2005, **105**, 1491–1546.
15 S. Sergeyev, W. Pisula and Y. H. Geerts, *Chem. Soc. Rev.*, 2007, **36**, 1902–1929.
16 X. Feng, W. Pisula and K. Müllen, *J. Am. Chem. Soc.*, 2007, **129**, 14116–14117.
17 X. L. Feng, J. S. Wu, M. Ai, W. Pisula, L. J. Zhi, J. P. Rabe and K. Müllen, *Angew. Chem., Int. Ed.*, 2007, **46**, 3033–3036.
18 X. Feng, V. Marcon, W. Pisula, M. R. Hansen, J. Kirkpatrick, F. Grozema, D. Andrienko, K. Kremer and K. Müllen, *Nat. Mater.*, 2009, **8**, 421–426.
19 R. Chesterfield, J. McKeen, C. Newman, P. Ewbank, D. da Silva, J. Bredas, L. Miller, K. Mann and C. Frisbie, *J. Phys. Chem. B*, 2004, **108**, 19281–19292.
20 J. Kim, I. Chung, Y. Kim and J. Yu, *Chem. Phys. Lett.*, 2004, **398**, 367–371.
21 C. Struijk, A. Sieval, J. Dakhorst, M. van Dijk, P. Kimkes, R. Koehorst, H. Donker, T. Schaafsma, S. Picken, A. van de Craats, J. Warman, H. Zuilhof and E. Sudholter, *J. Am. Chem. Soc.*, 2000, **122**, 11057–11066.
22 P. Malenfant, C. Dimitrakopoulos, J. Gelorme, L. Kosbar, T. Graham, A. Curioni and W. Andreoni, *Appl. Phys. Lett.*, 2002, **80**, 2517–2519.
23 J. J. M. Halls and R. H. Friend, *Synth. Met.*, 1997, **85**, 1307–1308.
24 C. Im, W. Tian, H. Bassler, A. Fechtenkotter, M. Watson and K. Müllen, *Synth. Met.*, 2003, **139**, 683–686.
25 I. A. Howard, F. Laquai, P. E. Keivanidis, R. H. Friend and N. C. Greenham, *J. Phys. Chem. C*, 2009, **113**, 21225–21232.
26 B. Jones, M. Ahrens, M. Yoon, A. Facchetti, T. Marks and M. Wasielewski, *Angew. Chem., Int. Ed.*, 2004, **43**, 6363–6366.
27 F. Nolde, W. Pisula, S. Müller, C. Kohl and K. Müllen, *Chem. Mater.*, 2006, **18**, 3715.
28 Z. J. Chen, V. Stepanenko, V. Dehm, P. Prins, L. D. A. Siebbeles, J. Seibt, P. Marquetand, V. Engel and F. Würthner, *Chem.–Eur. J.*, 2007, **13**, 436–449.
29 X. Zhang, Z. Chen and F. Würthner, *J. Am. Chem. Soc.*, 2007, **129**, 4886.
30 F. Würthner, *Chem. Commun.*, 2004, 1564–1579.
31 A. van de Craats, J. Warman, P. Schlichting, U. Rohr, Y. Geerts and K. Müllen, *Synth. Met.*, 1999, **102**, 1550–1551.
32 Z. Chen, V. Stepanenko, V. Dehm, P. Prins, L. D. A. Siebbeles, J. Seibt, P. Marquetand, V. Engel and F. Würthner, *Chem.–Eur. J.*, 2007, **13**, 436.
33 I. McCulloch, M. Heeney, M. Chabinyc, D. DeLongchamp, R. Kline, M. Coelle, W. Duffy, D. Fischer, D. Gundlach, B. Hamadani, R. Hamilton, L. Richter, A. Salleo, M. Shkunov, D. Sporrowe, S. Tierney and W. Zhong, *Adv. Mater.*, 2009, **21**, 1091–1109.
34 A. van de Craats, J. Warman, A. Fechtenkotter, J. Brand, M. Harbison and K. Müllen, *Adv. Mater.*, 1999, **11**, 1469–1472.
35 H. Sirringhaus, P. J. Brown, R. H. Friend, M. M. Nielsen, K. Bechgaard, B. M. W. Langeveld-Voss, A. Spiering, R. Janssen, E. Meijer, P. Herwig and D. de Leeuw, *Nature*, 1999, **401**, 685–688.
36 Y. Kim, S. Cook, S. Tuladhar, S. Choulis, J. Nelson, J. Durrant, D. Bradley, M. Giles, I. Mcculloch, C. Ha and M. Ree, *Nat. Mater.*, 2006, **5**, 197–203.
37 A. M. vande Craats, J. M. Warman, A. Fechtenkötter, J. D. Brand, M. A. Harbison and K. Müllen, *Adv. Mater.*, 1999, **11**, 1469–1472.
38 A. Fechtenkötter, K. Saalwaechter, M. A. Harbison, K. Müllen and H. W. Spiess, *Angew. Chem., Int. Ed.*, 1999, **38**, 3039–3042.
39 M. G. Debije, J. Piris, M. P. de Haas, J. M. Warman, Z. Tomovic, C. D. Simpson, M. D. Watson and K. Müllen, *J. Am. Chem. Soc.*, 2004, **126**, 4641–4645.
40 M. Kastler, W. Pisula, F. Laquai, A. Kumar, R. J. Davies, S. Baluschev, M. C. Garcia-Gutierrez, D. Wasserfallen, H. J. Butt, C. Riekel, G. Wegner and K. Müllen, *Adv. Mater.*, 2006, **18**, 2255.
41 W. Pisula, M. Kastler, D. Wasserfallen, M. Mondeshki, J. Piris, I. Schnell and K. Müllen, *Chem. Mater.*, 2006, **18**, 3634–3640.
42 D. W. Breiby, O. Bunk, W. Pisula, T. I. Solling, A. Tracz, T. Pakula, K. Müllen and M. M. Nielsen, *J. Am. Chem. Soc.*, 2005, **127**, 11288–11293.
43 D. Breiby, F. Hansteen, W. Pisula, O. Bunk, U. Kolb, J. Andreasen, K. Müllen and M. Nielsen, *J. Phys. Chem. B*, 2005, **109**, 22319–22325.
44 C. Ochsenfeld, *Phys. Chem. Chem. Phys.*, 2000, **2**, 2153–2159.
45 C. Ochsenfeld, S. P. Brown, I. Schnell, J. Gauss and H. W. Spiess, *J. Am. Chem. Soc.*, 2001, **123**, 2597–2606.
46 M. R. Hansen, R. Graf, S. Sekharan and D. Sebastiani, *J. Am. Chem. Soc.*, 2009, **131**, 5251–5256.
47 J. Kirkpatrick, V. Marcon, J. Nelson, K. Kremer and D. Andrienko, *Phys. Rev. Lett.*, 2007, **98**, 227402.
48 J. Kirkpatrick, V. Marcon, K. Kremer, J. Nelson and D. Andrienko, *J. Chem. Phys.*, 2008, **129**, 094506.
49 G. Cinacchi, R. Colle and A. Tani, *J. Phys. Chem. B*, 2004, **108**, 7969–7977.
50 V. Marcon, T. Vehoff, J. Kirkpatrick, C. Jeong, D. Y. Yoon, K. Kremer and D. Andrienko, *J. Chem. Phys.*, 2008, **129**, 094505.
51 V. Marcon, J. Kirkpatrick, W. Pisula and D. Andrienko, *Phys. Status Solidi B*, 2008, **245**, 820–824.
52 S. Athanasopoulos, J. Kirkpatrick, D. Martinez, J. Frost, C. Foden, A. Walker and J. Nelson, *Nano Lett.*, 2007, **7**, 1785–1788.
53 J. Kirkpatrick, V. Marcon, J. Nelson and D. Andrienko, *Phys. Status Solidi B*, 2008, **245**, 835–838.
54 J. J. Kwiatkowski, J. Nelson, H. Li, J. L. Bredas, W. Wenzel and C. Lennartz, *Phys. Chem. Chem. Phys.*, 2008, **10**, 1852–1858.

55 Y. Nagata and C. Lennartz, *J. Chem. Phys.*, 2008, **129**, 034709.
56 D. L. Cheung and A. Troisi, *Phys. Chem. Chem. Phys.*, 2008, **10**, 5941–5952.
57 A. Troisi, D. L. Cheung and D. Andrienko, *Phys. Rev. Lett.*, 2009, **102**, 116602.
58 J. Nelson, J. Kwiatkowski, J. Kirkpatrick and J. Frost, *Acc. Chem. Res.*, 2009, **42**, 1768–1778.
59 A. Lukyanov and D. Andrienko, *Phys. Rev. B: Condens. Matter Mater. Phys.*, 2010, **82**, 193202.
60 T. Vehoff, B. Baumeier and D. Andrienko, *J. Chem. Phys.*, 2010, **133**, 134901.
61 T. Vehoff, B. Baumeier, A. Troisi and D. Andrienko, *J. Am. Chem. Soc.*, 2010, **132**, 11702–11708.
62 M. R. Hansen, T. Schnitzler, W. Pisula, R. Graf, K. Müllen and H. W. Spiess, *Angew. Chem., Int. Ed.*, 2009, **48**, 4621–4624.
63 I. Schnell and H. W. Spiess, *J. Magn. Reson.*, 2001, **151**, 153–227.
64 S. P. Brown and H. W. Spiess, *Chem. Rev.*, 2001, **101**, 4125–4155.
65 S. P. Brown, *Prog. Nucl. Magn. Reson. Spectrosc.*, 2007, **50**, 199–251.
66 S. P. Brown, *Macromol. Rapid Commun.*, 2009, **30**, 688–716.
67 M. Feike, D. E. Demco, R. Graf, J. Gottwald, S. Hafner and H. W. Spiess, *J. Magn. Reson., Ser. A*, 1996, **122**, 214–221.
68 M. Feike, R. Graf, I. Schnell, C. Jager and H. W. Spiess, *J. Am. Chem. Soc.*, 1996, **118**, 9631–9634.
69 K. Saalwächter and I. Schnell, *Solid State Nucl. Magn. Reson.*, 2002, **22**, 154–187.
70 I. Schnell, S. Brown, H. Low, H. Ishida and H. W. Spiess, *J. Am. Chem. Soc.*, 1998, **120**, 11784–11795.
71 J. Schmidt, A. Hoffmann, H. W. Spiess and D. Sebastiani, *J. Phys. Chem. B*, 2006, **110**, 23204–23210.
72 V. Marcon, D. W. Breiby, W. Pisula, J. Dahl, J. Kirkpatrick, S. Patwardhan, F. Grozema and D. Andrienko, *J. Am. Chem. Soc.*, 2009, **131**, 11426–11432.
73 J. R. Yates, T. N. Pham, C. J. Pickard, F. Mauri, A. M. Amado, A. M. Gil and S. P. Brown, *J. Am. Chem. Soc.*, 2005, **127**, 10216–10220.
74 A.-C. Uldry, J. M. Griffin, J. R. Yates, M. Perez-Torralba, M. D. S. Maria, A. L. Webber, M. L. L. Beaumont, A. Samoson, R. M. Claramunt, C. J. Pickard and S. P. Brown, *J. Am. Chem. Soc.*, 2008, **130**, 945–954.
75 N. Tasios, C. Grigoriadis, M. R. Hansen, H. Wonneberger, C. Li, H. W. Spiess, K. Mllen and G. Floudas, *J. Am. Chem. Soc.*, 2010, **132**, 7478–7487.
76 E. Lindahl, B. Hess and D. van der Spoel, *J. Mol. Mod.*, 2001, **7**, 306–317.
77 V. Rühle, C. Junghans, A. Lukyanov, K. Kremer and D. Andrienko, *J. Chem. Theory Comput.*, 2009, **5**, 3211–3223.
78 R. A. Marcus, *Rev. Mod. Phys.*, 1993, **65**, 599.
79 G. R. Hutchison, M. A. Ratner and T. J. Marks, *J. Am. Chem. Soc.*, 2005, **127**, 2339.
80 V. Lemaur, D. Da Silva Filho, V. Coropceanu, M. Lehmann, Y. Geerts, J. Piris, M. Debije, A. Van de Craats, K. Senthilkumar, L. Siebbeles, J. Warman, J. Bredas and J. Cornil, *J. Am. Chem. Soc.*, 2004, **126**, 3271–3279.
81 B. Baumeier, D. Andrienko and J. Kirkpatrick, *Phys. Chem. Chem. Phys.*, 2010, **12**, 11103–11113.